Porous photonic crystal external cavity laser biosensor

Qinglan Huang, Jessie Peh, Paul J. Hergenrother, and Brian T. Cunningham

Citation: Appl. Phys. Lett. **109**, 071103 (2016); doi: 10.1063/1.4961107
View online: http://dx.doi.org/10.1063/1.4961107
View Table of Contents: http://aip.scitation.org/toc/apl/109/7
Published by the American Institute of Physics

Porous photonic crystal external cavity laser biosensor

Qinglan Huang,[1] Jessie Peh,[2] Paul J. Hergenrother,[2] and Brian T. Cunningham[1,3]
[1]Department of Electrical and Computer Engineering, University of Illinois at Urbana-Champaign, Urbana, Illinois 61801, USA
[2]Department of Chemistry, University of Illinois at Urbana-Champaign, Urbana, Illinois 61801, USA
[3]Department of Bioengineering, University of Illinois at Urbana-Champaign, Urbana, Illinois 61801, USA

(Received 28 May 2016; accepted 30 July 2016; published online 15 August 2016)

We report the design, fabrication, and testing of a photonic crystal (PC) biosensor structure that incorporates a porous high refractive index TiO_2 dielectric film that enables immobilization of capture proteins within an enhanced surface-area volume that spatially overlaps with the regions of resonant electromagnetic fields where biomolecular binding can produce the greatest shifts in photonic crystal resonant wavelength. Despite the nanoscale porosity of the sensor structure, the PC slab exhibits narrowband and high efficiency resonant reflection, enabling the structure to serve as a wavelength-tunable element of an external cavity laser. In the context of sensing small molecule interactions with much larger immobilized proteins, we demonstrate that the porous structure provides 3.7× larger biosensor signals than an equivalent nonporous structure, while the external cavity laser (ECL) detection method provides capability for sensing picometer-scale shifts in the PC resonant wavelength caused by small molecule binding. The porous ECL achieves a record high figure of merit for label-free optical biosensors. *Published by AIP Publishing.*
[http://dx.doi.org/10.1063/1.4961107]

Screening through chemical compound libraries comprised of millions of small molecules for their potential to specifically interact with target proteins that represent key elements of disease biomolecular pathways is one of the most important methods through which new potential drugs are initially discovered.[1] Due to their low molecular weight (150–500 Da), low analyte concentration, 1:1 binding stoichiometry, and (often) low binding affinities, the ability to rapidly characterize small molecule binding with much larger proteins (20–150 kDa) remains an important technical challenge.[2] Label-free biosensors based upon measuring wavelength shifts of optical resonators have been used effectively for characterizing biomolecular interactions using technologies that include surface plasmon resonance,[3] photonic crystal (PC) biosensors,[4] optical fibers,[5] waveguides,[6] and interferometers.[7] The performance of these approaches can be quantified by a figure of merit[8] (FOM) defined as $FOM = S_b \cdot Q/\lambda_0$, where the sensitivity $S_b = \frac{\Delta\lambda}{\Delta n}$ characterizes the magnitude of the output shift induced by a known bulk refractive index (RI) change, and Q/λ_0 is the full width at half maximum (FWHM) of the resonant spectrum that describes the spectral resolving ability. While several recently reported label-free optical biosensing approaches seek to maximize the Q-factor ($Q = \lambda_0/FWHM$) of passive resonators,[9,10] the increased detection resolution is achieved at the expense of reduced S_b, as the resonant electric fields reside within solid internal regions of the biosensor structure, while biomolecular binding occurs only on the structure's outer surface.

The External Cavity Laser (ECL) biosensor is a fundamentally different instrumentation approach that can achieve both high sensitivity and high Q-factor simultaneously[11] and has been demonstrated in conjunction with PC biosensors for pharmaceutical high-throughput screening (HTS) with high specificity and sub-picometer accuracy.[12] Briefly, the stimulated emission of a semiconductor optical amplifier (SOA) generates extremely narrowband optical output ($Q = 2.8 \times 10^7$), by incorporating a PC resonator as the tunable element of an external cavity laser. The ECL biosensor decouples the Q-factor from the biosensor's sensitivity by introducing external optical gain (i.e., SOA which is external to the transducer PC), allowing high resolution without compromising sensitivity. The ECL biosensor differs from the distributed feedback (DFB) laser biosensor[13] through the establishment of external laser cavity, where photons circulate and achieve continuous-wave operation with higher Q factor. Meanwhile, the electrically pumped SOA possesses greater single mode lasing stability and better temperature control than a chemical dye that resides within the sensor structure. While detection of small molecules has not been demonstrated using a DFB laser biosensor, the ECL approach shown in this work is capable of sensing small molecules binding to immobilized proteins with high signal-to-noise ratio. While previous reports of PC-ECL biosensing were achieved with solid dielectric PC biosensor surfaces upon which biomolecular binding only occurred on the outer surface, here we report utilization of a porous PC biosensor in which a nanorod TiO_2 layer is used to improve sensitivity by ∼4×, while lasing linewidth remains 0.03 pm. The approach demonstrates a $FOM = 1.05 \times 10^7$, representing the highest values for an optical biosensor yet reported. See Table S1 in the supplementary material for FOM comparison among a list of recently reported optical biosensors. In this work, we discuss the design and operating principle of the sensor structure, describe the use of the sensor in a self-referencing ECL detection instrument, characterize the S_b and Q-factor performance, and demonstrate kinetic sensing of a representative small molecule drug-protein interaction.

The porous PC is a one-dimensional grating structure fabricated on a low refractive index, ultra-violet curable polymer (UVCP) ($\Lambda = 550$ nm, $t_{grating} = 170$ nm, $n = 1.5$), which is

coated with two layers of TiO_2 thin films (Fig. 1(a)). Following the sputtering of the first solid TiO_2 layer ($n = 2.4$, $d_{TiO_2} = 75$ nm), a layer of porous TiO_2 film is formed by glancing angle deposition (GLAD).[14] As shown in the scanning electron microscopic images of the top (Fig. 1(b)) and cross-sectional (Fig. 1(c)) views of the device, the porous layer is a uniform sheet of tilted TiO_2 nanorods with a height of ~80 nm and a lean angle of ~35°. Next, dry etch using CF_4 (PlasmaLab Freon RIE) is performed to slightly expand the gaps between TiO_2 nanorods.[15] The etch step is important, as gaps between nanorods of $\gtrsim$20 nm are required to enable protein molecules to diffuse into the pores and to bind within the structure, rather than simply attaching to the upper surface of the porous layer. Fig. S3 in the supplementary material shows how the porosity is controlled during device fabrication and effects of porosity on experimental sensitivity. The porous PC is designed to function in aqueous media, with water perfused between nanorods. At resonance, the subwavelength grating couples the external incident light to excite a guided mode resonance (GMR) as described in previous reports.[16] The GMR, defined by a complex propagation constant, possesses a finite lifetime and is re-radiated into free space to form a narrow band reflection. Therefore, the near-field electromagnetic (EM) field enhancement is associated with a far-field resonant reflection peak. As shown in the reflection spectrum in Fig. 1(d), the porous PC reflects a narrow range of wavelengths centered at $\lambda = 851$ nm, with FWHM = 5 nm. Because the features of the nanorods are far smaller than the resonant wavelength, the nanorod layer does not cause scattering or absorption that results in extinguishing the resonance.[14] Compared with non-porous PCs, the porous PCs do not result in significant broadening or shortening of the resonant peak, which is vital to establishing lasing action in the ECL system.

The resonant reflection wavelength is modified by the absorption of biomolecules on the sensor surface and within the porous layer. At resonance, energy associated with the light is temporarily stored in the resonator and the surrounding medium in the form of an electromagnetic standing wave with an evanescent reduction in intensity as one moves in the z-direction into the media. The resonant fields induce dipole moments in biomolecules within the evanescent field volume. As bound proteins and small molecules displace water, we observe a shift in the photon energy of the resonant state.[10]

By first order perturbation theory, the fractional resonant wavelength shift from a large number of molecules bound on optical resonators can be estimated as the ratio of the energy needed to polarize and induce dipole moments in the molecules and the total energy of the mode[17]

$$\frac{\Delta\lambda}{\lambda} = \frac{\alpha_{ex}\sigma_p \int |\mathbf{E}(\mathbf{r})|^2 dA}{2\int \varepsilon |\mathbf{E}(\mathbf{r})|^2 dV}, \tag{1}$$

where α_{ex} is the molecules' excess polarizability to water, σ_p is the protein surface density, A is the surface area where binding events occur, and V is the mode volume. Eq. (1) relates to the experiments in two aspects. First, it describes how a porous surface increases the sensitivity from the perspective of the overlap of the resonant electromagnetic field with the spatial locations where biomolecular binding occurs. Second, (1) estimates the relative resonant shift magnitude enhancement of a porous versus a nonporous PC, which correlates well with the experimental results. The porous PC boosts sensitivity by simultaneously increasing the integral area and modifying the electric field intensity profile. First, the nanorods extrude the originally flat surface into a three-dimensional (3D) volume within the evanescent

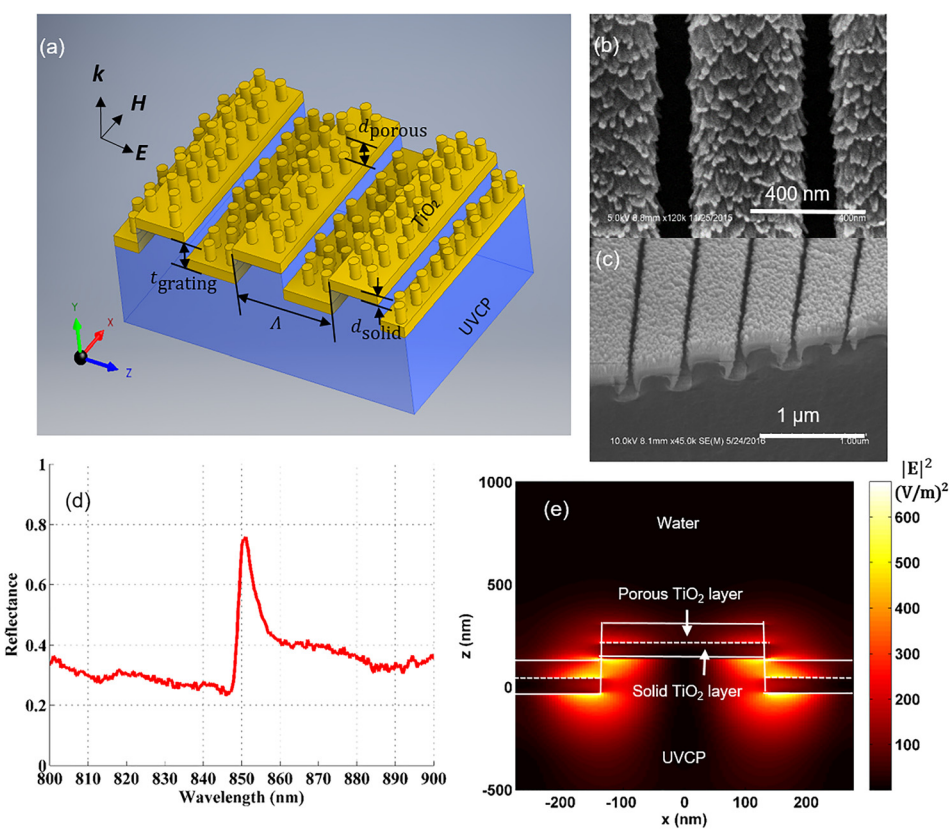

FIG. 1. Porous photonic crystals. (a) Schematic diagram of the porous PC structure, together with the polarization and orientation of incident light. Scanning electron microscopic images of the (b) top and (c) cross-sectional views of the porous PC. (d) Measured reflection spectrum when the porous PC is covered with water, with TM-polarized normal incident light. (e) FDTD computed near electric field intensity profile $|\mathbf{E}|^2$ for normally unit incident plain wave for the TM resonant mode at $\lambda = 851$ nm.

field region and increase the surface area.[18] We estimate a surface enhancement factor as follows. With the measured refractive index (RI) of the porous layer 1.40, which is the weighted average RI of TiO_2 and air in space, the volume ratio of the two materials can be approximated as 0.3:0.7. Then, nanorods can be approximated as an array of 40 nm diameter cylinders with 25 nm wide gaps and 80 nm height. Compared to a flat surface, the extra surface area provided by cylinder sidewalls can be calculated. Thus, a maximum 3.4× enhancement in the surface area is expected. However, because protein molecules occupy 3D volumes that will prevent close-packed occupation of all the available surface area (for example, two proteins may not fit in one gap between neighboring rods), we cannot expect the surface area enhancement to correlate precisely with the density of immobilized capture proteins in the structure. The extended surface area is accompanied by efficient projection of the evanescent field onto the biomolecule binding volume. The resonant electric field intensity profile calculated by the finite difference time domain (FDTD) method (Lumerical) is shown in Fig. 1(e), where the porous layer is modeled as a uniform dielectric layer with measured RI of the layer. The evanescent field tail extends to ∼200 nm above the sensor surface and overlaps with the porous layer. Each location in the porous 3D biomolecule binding volume contributes to tuning the resonance wavelength, whereas in the non-porous PCs, only the electric field within a 30 nm-thin conformal sheet covering the PC surface interacts with the biomolecules, and a large portion of the evanescent field above the 30 nm threshold does not participate in biosensing.

Second, the porous layer modifies the resonant mode profile and increases the electric field intensity especially in the porous layer, enlarging the numerator in (1). This can be shown by comparing the near field of the porous PC (Fig. 1(e)) and nonporous PC (Fig. S1 in the supplementary material shows the field profile of the nonporous PC). The porous PC provides higher electric field intensity than nonporous PC. Meanwhile, with a porous layer, the evanescent field extends to a considerably larger volume above the solid dielectric. The absolute shift value can be estimated from (1) if the E field magnitude is known everywhere in the porous layer. In our FDTD model, to save computation resources, the discrete TiO_2 nanorods and water pores in between are not taken into account, instead a uniform RI layer is used to represent the weighted average of TiO_2 and water. This configuration reflects the resonant spectrum and coarse mode distribution but does not provide nanometer-scale spatial resolution of the E field magnitude in the TiO_2 nanorods and in the water pores in between. To demonstrate this phenomenon experimentally, we compare the bulk refractive sensitivity of the porous and non-porous PCs. By exposing each PC surface to a series of water: DMSO (Dimethyl sulfoxide) mixtures over a range of DMSO concentrations, we determine the bulk sensitivity of the porous PC to be 316 nm/RIU, while the bulk sensitivity of a non-porous PC is 212 nm/RIU. The bulk sensitivity comparison is shown in Fig. S2 in the supplementary material. Therefore, the field profile mechanism contributes to approximately 1.5× the wavelength shift induced for a fixed change in dielectric permittivity for the material added to the sensor surface or porous volume.

Next, we demonstrate the lasing ability of the ECL system based on porous PCs. The ECL cavity, as depicted in Fig. 2(a), is formed by the porous PC resonant reflector and a broadband mirror, where the porous PC serves as a wavelength selective element. Optical gain is provided by the fiber coupled SOA (SAL-372, Superlum Inc., $\lambda_0 = 850$ nm and a 3-dB bandwidth of $\Delta\lambda = 40$ nm). The light coming from one end of the fiber is reflected against the mirror, while light from the other output of the SOA is directed by a collimator to illuminate two adjacent sensors at normal incidence from below. The polarization of the incident light from the polarizing maintaining (PM) fiber is adjusted so that the s- and p- polarized light from the polarizing beam splitter (PBS) have equal intensity. The half-wave plate ensures that both beams are polarized perpendicular to the PC gratings. The reflection of the porous PC is coupled back into the laser cavity, where it is amplified by the SOA. An active optical resonator with two resonant modes is established through the stimulated emission process, and a shutter alternates between excitation of the "active" and "reference" sensor. The reference sensor is identical to the active sensor but is not prepared with an immobilized protein. The dual-mode operation provides self-referencing to compensate for the common noise sources including thermal fluctuation and non-specific binding.[12,19] The noise level is calibrated as a standard deviation of 0.8 pm over a 20 min period, when both sensors are covered with water. The mode spacing of 0.08 pm (Ref. 11) ensures continuous tuning of lasing wavelength without abrupt hops between modes. The fiber coupler couples 1% of the light from the cavity to LabVIEW-controlled dual-measurement instruments to monitor binding events in real time. A spectrum analyzer (Model 721, Bristol

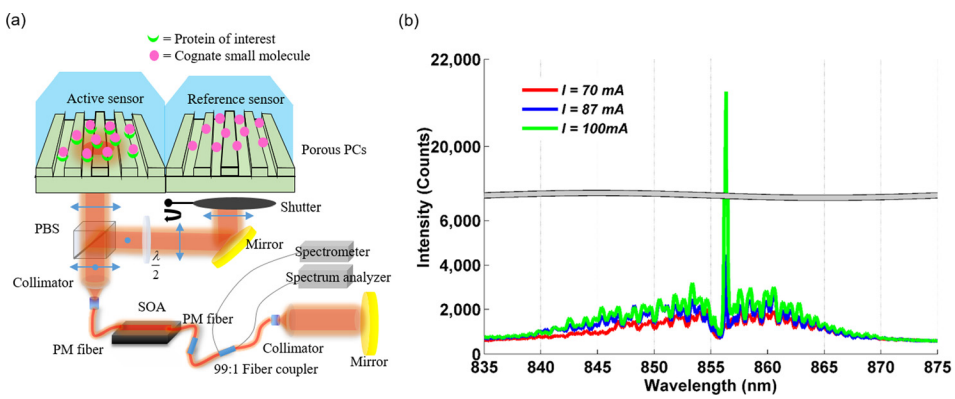

FIG. 2. Porous PC external cavity laser. (a) Schematic diagram of the external cavity laser biosensor system. A pulse driven bistable shutter enables alternate operation of the "active" and "reference" lasing mode with 0.5 Hz frequency. (b) Spectra of the ECL system output light (collected from above a porous PC sensor) with injection current under (red), just above (blue), and well above (green) the threshold. Here, the porous PC is immersed in water: DMSO solution.

Instruments, Inc., 0.2 pm resolution) tracks the peak lasing wavelength. We implement repeated testing of the laser wavelength value (LWV), in which serial N (=10 in this work) independent LWV measurements taken at 50 ms intervals are averaged to generate a "final" LWV with a resolution of 0.2 pm/$N^{1/2}$ (~0.06 pm). A spectrometer (HR 4000, Ocean optics, 20 pm resolution) enables observation of the spectrum to verify single mode operation.

The lasing wavelength depends on the first longitudinal mode that achieves the threshold condition and is tuned by the absorption of biomolecules on the PC surface. The output spectra of the ECL system collected from the above sensors, shown in Fig. 2(b), clearly demonstrate the porous PCs' wavelength selection function. The raised background represents the broadband SOA spontaneous emission, where the porous PC resonance registers a transmission dip at the center of the SOA gain spectrum near $\lambda = 855$ nm. The dynamics of establishing lasing behavior is illustrated by three curves, representing the output below (red), just above (blue), and well above (green) the lasing threshold, respectively. Above the threshold, a laser emission occurs at the valley, overlapping with the porous PC resonance. The relative broad PC resonant reflection peak translates into a narrow laser emission spike via the process of stimulated emission. The laser output surpasses the spontaneous emission and gradually increases intensity with increasing injection current. The laser output power is approximately 1 mW, which is considerably lower than passive WGM biosensors[20] or other active pulse pumped optical sensors.[13] A precise calibration of the ECL laser emission using a scanning Fabry–Pérot interferometer demonstrated single-mode lasing with a FWHM of 0.03 pm.[11] The narrow linewidth enables resonant wavelength shifts to be resolved with sub-picometer accuracy. Therefore, the porous ECL establishes a record high FOM of 1.05×10^7.

To demonstrate the improved sensitivity in biosensing, we compare the response of both porous and non-porous PCs to the interactions of a well-characterized protein-small molecule binding pair: Carbonic Anhydrase-II (CA II, MW = 29 kDa) and drug molecule dorzolamide (MW = 324 Da) with a dissociation constant of $K_D = 1.1$ nM.[12] Both sensors undergo the same three-step assay to immobilize the protein CA II onto the surface, which has been described in previously published work.[12,14] Each of the sensor surface chemistry preparation steps, in which the sensors are treated in sequence with polyvinylamine (PVA, provided by SRU Biosystems Inc.)–Glutaraldehyde (GA), and CA II generates ~4× larger laser wavelength value (LWV) shifts in porous PCs as compared to non-porous PCs (Fig. 3(a)). The error bars represent the standard deviation of three identical sensors measured independently for each condition. This result indicates higher sensitivity for the porous PCs, and higher density of capture proteins immobilized on the porous PCs. Next, the porous and non-porous PCs are exposed to 50 μM of dorzolamide, using a concentration well above the K_D value, so as to saturate the available binding sites on immobilized CA II. Because our system does not utilize microfluidic flow (the liquid in contact with the sensor is static), the kinetic binding characteristic measured is limited by diffusion of molecules to the biosensor surface, rather than by the chemical binding interaction that is typically used to measure K_D. Therefore, we cannot estimate K_D from the biosensor measurements shown in this paper. We intentionally provide a small molecule concentration in excess of K_D to ensure that all the available protein binding sites can be saturated with small molecule analyte, as in done in the context of small molecule screening, which is the intended application for this technology. The kinetic LWV shift as a function of time for both sensors is shown in Fig. 3(b). A LWV shift of 52 pm is observed in the porous PCs, while a shift of only 14 pm occurs in the non-porous PCs. The 3.7× enhancement in the wavelength shift corresponds well with the wavelength shift enhancement in the surface chemistry steps and is expected due to the 1:1 binding stoichiometry of dorzolamide to its attachment site on the CA II protein. Both curves are the difference between the LWV shifts in the active and reference wells and represent the "net" signals associated with actual biomolecule binding. Both resonant shifts induced by dorzolamide are greater than three standard deviations (3σ) of the noise. This result shows the considerably higher signal-to-noise ratio and sensitivity offered by the porous PCs. The 3.7× enhanced wavelength shift magnitude difference between the two types of PCs occurs by a combination of enhanced surface area (which results in more CA II

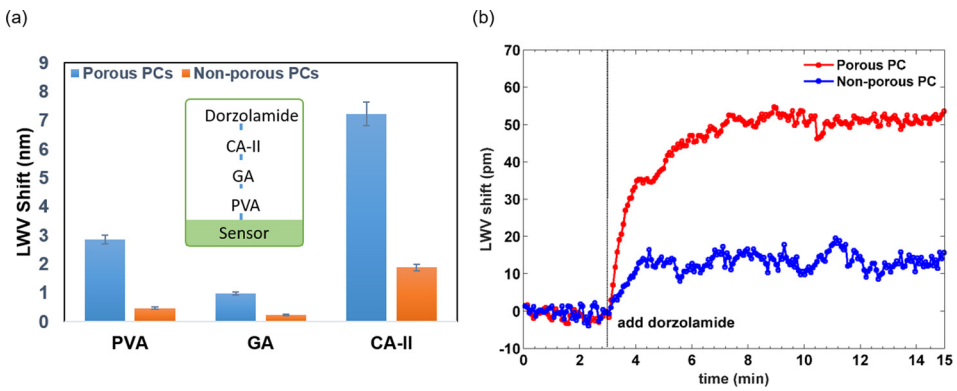

FIG. 3. Improved sensitivity of the porous PCs as compared to non-porous PCs. (a) Laser wavelength value (LWV) shifts for porous and non-porous PCs after each step of the surface chemistry process. The error bars represent the standard deviation of three independent sensors. Inset: illustration of the four-step assay to test CA II–dorzolamide binding. (b) Observed kinetic LWV shift for the CA II–dorzolamide interaction, for the porous PC (red) and non-porous PC (blue) sensors. The vertical dotted line indicates the addition of dorzolamide to both the active and reference wells.

capture protein immobilized within the porous TiO_2 than the density of capture protein that can bind upon a "flat" non-porous layer) and greater interaction between the PC resonant mode and the volume in which biomolecules attach, which we characterized as a $\sim 1.5\times$ sensitivity enhancement via the bulk refractive index sensitivity.

In conclusion, a nanorod-coated porous PC was designed and fabricated for use in conjunction with an ECL biosensor detection instrument to kinetically detect protein-small molecule binding interactions. The porous PCs deliver $3.7\times$ higher sensitivity than non-porous sensors through a combination of their enhanced surface area and effective utilization of the evanescent field. With the porous PC functioning as a wavelength selective element in the ECL, this optical label-free biosensor achieves a record high FOM of 1.05×10^7. Kinetic monitoring of a small molecule drug interacting with an immobilized target protein was performed to verify the performance of the porous PC-ECL system for a representative assay used in pharmaceutical high throughput screening. For passive high-Q optical resonators, a higher Q-factor directly translates into greater difficulty of coupling light into the structure, in terms of the range of allowable conditions (such as wavelength or coupling angle) that can generate a sustained optical standing wave. The ECL biosensor provides excellent robustness from the standpoint that the sensor does not require stringent alignment conditions to the illumination source, and that the output of the system can be measured easily with a simple instrument.

See supplementary material for experimental details and supporting data.

The work was supported by the National Institutes of Health (NIH R01 GM090220). We gratefully acknowledge Jui-Nung Liu (UIUC) and Meng Zhang (UIUC).

[1]J. Drews, Science **287**(5460), 1960 (2000).
[2]W. U. Wang, C. Chen, K.-h. Lin, Y. Fang, and C. M. Lieber, Proc. Natl. Acad. Sci. U.S.A. **102**(9), 3208 (2005).
[3]S. Szunerits and R. Boukherroub, Chem. Commun. **48**(72), 8999 (2012).
[4]B. T. Cunningham, M. Zhang, Y. Zhuo, L. Kwon, and C. Race, IEEE Sens. J. **16**(10), 3349 (2016).
[5]K. H. Smith, B. L. Ipson, T. L. Lowder, A. R. Hawkins, R. H. Selfridge, and S. M. Schultz, Appl. Opt. **45**(8), 1669 (2006).
[6]M. Zourob, S. Mohr, B. J. Treves Brown, P. R. Fielden, M. B. McDonnell, and N. J. Goddard, Anal. Chem. **77**(1), 232 (2005).
[7]A. Ymeti, J. S. Kanger, J. Greve, P. V. Lambeck, R. Wijn, and R. G. Heideman, Appl. Opt. **42**(28), 5649 (2003).
[8]M. Zhang, M. Lu, C. Ge, and B. T. Cunningham, Opt Express **22**(17), 20347 (2014).
[9]J. T. Gohring, P. S. Dale, and X. Fan, Sens. Actuators, B **146**(1), 226 (2010); M. Iqbal, M. A. Gleeson, B. Spaugh, F. Tybor, W. G. Gunn, M. Hochberg, T. Baehr-Jones, R. C. Bailey, and L. C. Gunn, IEEE J. Sel. Top. Quantum Electron. **16**(3), 654 (2010).
[10]F. Vollmer, D. Braun, A. Libchaber, M. Khoshsima, I. Teraoka, and S. Arnold, Appl. Phys. Lett. **80**(21), 4057 (2002).
[11]C. Ge, M. Lu, S. George, T. A. Flood, C. Wagner, J. Zheng, A. Pokhriyal, J. G. Eden, P. J. Hergenrother, and B. T. Cunningham, Lab Chip **13**(7), 1247 (2013).
[12]M. Zhang, J. Peh, P. J. Hergenrother, and B. T. Cunningham, J. Am. Chem. Soc. **136**(16), 5840 (2014).
[13]C. Ge, M. Lu, W. Zhang, and B. T. Cunningham, Appl. Phys. Lett. **96**(16), 163702 (2010).
[14]W. Zhang, N. Ganesh, I. D. Block, and B. T. Cunningham, Sens. Actuators, B **131**(1), 279 (2008).
[15]M. R. Kupsta, M. T. Taschuk, M. J. Brett, and J. C. Sit, IEEE Sens. J. **9**(12), 1979 (2009).
[16]N. Ganesh, W. Zhang, P. C. Mathias, E. Chow, J. A. N. T. Soares, V. Malyarchuk, A. D. Smith, and B. T. Cunningham, Nat. Nanotechnol. **2**(8), 515 (2007).
[17]S. Arnold, M. Khoshsima, I. Teraoka, S. Holler, and F. Vollmer, Opt. Lett. **28**(4), 272 (2003).
[18]W. Zhang, S.-m. Kim, N. Ganesh, I. D. Block, P. C. Mathias, H.-Y. Wu, and B. T. Cunningham, J. Vac. Sci. Technol. A **28**(4), 996 (2010).
[19]M. Zhang, C. Ge, M. Lu, Z. Zhang, and B. T. Cunningham, Appl. Phys. Lett. **102**(21), 213701 (2013).
[20]F. Vollmer and S. Arnold, Nat. Methods **5**(7), 591 (2008).